Event-chain Monte Carlo and the true self-avoiding walk

A. C. Maggs
CNRS UMR 7083, ESPCI Paris, Université PSL, 10 rue Vauquelin, 75005 Paris, France.[*]

We study the large-scale dynamics of event-chain Monte Carlo algorithms in one dimension, and their relation to the true self-avoiding walk. In particular, we study the influence of stress, and different forms of interaction on the equilibration and sampling properties of algorithms with global balance, but no local balance. We conclude that a variety of potentials, corresponding to different physical systems, display identical large-scale dynamics.

INTRODUCTION

Irreversible Monte Carlo algorithms that rely on global balance [1, 2], while not obeying the more restrictive criterion of detailed balance have had remarkable successes in the study of hard numerical problems such as the nature of ordered phases of two-dimensional fluids [3]. See [4] for a comparison between irreversible and conventional algorithms in this context. A fundamental question is the origin of the acceleration of irreversible methods when compared to molecular dynamics and reversible Monte Carlo [5]. Such irreversible algorithms are rather unusual for dynamical systems sampling the equilibrium Boltzmann distribution. On-screen animations of simulations display large-scale coherent flows, in a manner that recalls active matter: Particles move in one direction giving a preferred orientation to motion. Despite this large-scale streaming, inter-particle collisions are finely tuned so that the flows do not disturb the equilibrium state. Indeed, it is because of this driven motion that irreversible methods explore configuration space more efficiently than diffusive algorithms such as Monte Carlo.

In a recent paper [6] we have demonstrated numerically that one irreversible algorithm, event-chain Monte Carlo (ECMC), applied to a harmonic chain is a realization of the so-called "true" self-avoiding walk [7–9]. This mapping allows us to understand the sampling properties of these new methods since analytic results are available characterizing the large-scale dynamics. The present paper is a continuation of [6] which can be consulted for more details as to the simulation methods. Code is available for the algorithms of both papers at [10].

The true self-avoiding walk was introduced, [7] as a dynamic model of polymer growth. On a lattice, monomers are added successively to a chain, avoiding places where the polymer has already passed. The probability of choosing a site i, which has already been visited $L_i(t)$ times is then

$$p_i(t+1) = \frac{e^{-\lambda L_i(t)}}{\sum_j e^{-\lambda L_j(t)}} \tag{1}$$

The sum is over all neighbors j of the current position at time t. $\lambda > 0$ is the strength of the repelling interaction. The large-scale behavior of the process is believed to be independent of λ, up to rescalings in space and time.

The original paper, introducing this growth process [7], postulates the existence of a continuum limit, described by coupled equations, here given in one spatial dimension

$$\frac{dX(t)}{dt} = -\partial_x L(t, x = X(t)) \tag{2}$$

$$\frac{dL(t,x)}{dt} = \delta(x - X(t)) \tag{3}$$

The function, $L(t,x)$, a *local time*, cumulates memory as to the occupation of the trajectory of the polymer end, $X(t)$. The local time in eq. (2) acts as a repulsive potential pushing the end of the growing polymer away from previously visited positions.

The mathematical literature on the true self-avoiding walk emphasizes the importance of two distribution functions. The first $\rho_1(t,x)$ describes the distribution of end-to-end separations, x, in a polymer growth problem. The second distribution $\rho_2(t,h)$ gives the distribution in the number of previous visits, h to the final position in the growth process. It was demonstrated that in the continuum limit,

$$\rho_1(t,x) = t^{-2/3}\nu_1(|x|t^{-2/3}) \tag{4}$$

$$\rho_2(t,h) = t^{-1/3}\nu_2(ht^{-1/3}) \tag{5}$$

where the scaling functions ν_1 and ν_2 are known [11–14]. They are plotted as solid, red lines in Fig. 8.

Event-chain Monte Carlo is implemented by using a single mobile (active) particle [2]. Motion is transferred to a new particle, with a generalized collision, using rules deduced from global balance (see below). We found numerically [6], that the integer index, i, of particles in a simulated chain can be scaled to the continuum variable x in eq. (2). Distribution functions found from the true self-avoiding walk and from event-chain Monte Carlo are remarkably similar. For instance, the distribution functions of the end-to-end separation of the growing polymer and the index of the final motile particle in an ECMC simulation both obey eq. (4) after scaling. Links to other physical processes are summarized in [15].

The detailed numerical comparisons we made considered only a tension-free harmonic chain, remaining close to the exact mathematical results. In this paper we consider a larger range of physical systems and potentials, and study the universality of our previous findings, trying to find situations where these results break down. It

[*] anthony.maggs@espci.fr

is clear that with general potentials this simple scaling form cannot appear: Eq. (4) is symmetric under $x \to -x$, so that the distribution of final positions of the mobile particle does not drift with time. In ECMC the position of the mobile (active) particle must drift with a constant speed [2], equal to the thermodynamic pressure, so that $\rho_1(t, x)$ cannot remain symmetric around the origin, $x = 0$ if the thermodynamic pressure of the simulation is non-zero. We will study how the distribution ρ_1 is modified by pressure by implementing ECMC in pre-stressed harmonic chains.

We then study non-harmonic interactions between particles, considering the case of exponential repulsion and Lennard-Jones interactions at low temperatures where typical snapshots show heterogeneous clustering. The drift (linked to the pressure) in the simulation of such systems can be canceled by modifying the microscopic interactions on a chain with the addition of an extra linear potential (factor field) [16]. This modified potential is built in such a way that it does not change the configurations generated, only the dynamics through the ECMC update rules. We thus modify the potential between two particles so that

$$V(r) \to V(r) + \bar{p}\, r \tag{6}$$

$\bar{p}$ is an estimate of the thermodynamic pressure, found in a short preliminary simulation. Remarkably, this modification was found to give rise to further acceleration in the sampling of the underlying physical system compared to classical ECMC. For the optimal choice of the amplitude of the linear potential (factor field) the dynamic exponent z, describing the relaxation of long-wavelength density fluctuations takes on the low value of $z = 1/2$, rather than the exponents $z = 1$ and $z = 2$ characteristic of molecular dynamics and Monte Carlo methods, and the value $z = 1$ characteristic of the historic ECMC method [16]. This acceleration is directly linked to the exponent 2/3, appearing in eq. (4). Indeed, the super-diffusive propagation displayed in eq. (4): $|x| \sim t^{2/3}$ is just linked via scaling to the dynamic exponent: $t \sim |x|^{(1+z)}$. We find that simulation of the modified potential eq. (6) brings the dynamics of exponential and Lennard-Jones potentials back into the universality class of the true self-avoiding walk.

In the following sections, we study several other properties of the ECMC method in one-dimensional systems. Firstly, we study the difference between cold and warm starts, finding the same universal function ρ_1. A recently introduced lattice model inspired by ECMC also has scaling properties identical to the true self-avoiding walk. This lifted TASEP [17] (Totally Asymmetric Simple Exclusion Process), corresponds to introducing a single mobile particle like in ECMC. The novelty in this model is a new collision rule that allows for backward motion of the mobile particle label, in a manner that is similar to the implementation of the factor field in ECMC. In this system we study a scaling ratio between ordered and random initial conditions and find the result is compatible with a universal ratio predicted [11] for the true self-avoiding walk for two different initial conditions for the continuum equations.

Finally, we break balance and study a non-equilibrium dynamical system, but find that characteristic singularities in the distribution function ρ_1 are still present.

IMPLEMENTATION OF IRREVERSIBLE ALGORITHMS

Our implementation of event-chain Monte Carlo follows the presentations of [6, 18]. The total potential energy of a physical system is broken up into a sum of independent factors. We take as factors the pair energy of particles in a chain. Motion of a single particle leads to changes in the pair energies, which is then used in an individualized Monte Carlo criterion (the factorized Metropolis algorithm) [19]. This individualized criterion allows one to choose a collision partner among all the changing interactions, and to continue the motion with a new mobile particle without generating a Monte Carlo rejection. The unique mobile particle at any moment is denoted "active". If the pair potential between two particles is $V(r)$ finding the candidate moment of collision, when motion is transferred to a new particle, requires solving an equation of the form

$$\Delta V^+(r) = -T \ln(\text{rand}) \tag{7}$$

rand is uniformly distributed on $(0, 1)$. $T = 1/\beta$ is the temperature. V^+ is constructed from a clipped derivative of V:

$$\frac{dV^+(r)}{dr} = \max\left(0, \frac{dV(r)}{dr}\right) \tag{8}$$

Eq. (7) corresponds to a variant of the Metropolis rule that rejects a trial when $\exp(-\beta\Delta V) <$ rand, for energy change ΔV. The solution to eq. (7) is the point of first rejection in Metropolis when working with the random number rand. One then compares all the candidate collisions and takes the very first; for a chain with nearest-neighbor interactions, this requires comparing two candidate events, coming from the two neighbors. The implementation is rendered more complicated because, in general, we are interested in the addition of a linear potential (factor field) [16] to the bare potential $V(r)$, eq. (6).

In this paper, we consider three cases. Firstly harmonic chains, where it is possible to find the solution to eq. (7) with elementary functions. Secondly, the case of exponentially repelling particles for which the Lambert-W function [20] allows a direct solution to the energy equation. Finally, the Lennard-Jones potential, for which we use iterative root solvers for eq. (7). The Lennard-Jones system is studied at a low temperature where the system breaks into small clusters so that the dynamics are highly heterogeneous, and are a harder test of universality.

These different models allow us to explore the universality of the distribution function $\rho_1(t,x)$ as well as test how to implement factor field acceleration in the case that interactions go beyond nearest neighbors. We explore interactions with first and second-nearest neighbors and show how to implement factor field acceleration in this more general system.

HARMONIC CHAINS

We first extend our study of the harmonic chain [6]. Our previous work only considered the dynamics of a system prepared in its ground state (cold starts). We now study the effects of temperature jumps on the dynamics.

We take as the energy

$$E = \frac{k}{2}\sum_{i=1}^{N}(y_i - y_{i+1})^2 \tag{9}$$

with $y_i \equiv y_{N+i}$. k is a spring constant. The quadratic energy function of a harmonic chain with nearest-neighbor interactions can be written in terms of a sparse (mostly zero-filled) matrix, $E = y^T My/2$. This matrix M, admits a Cholesky factorization, $M = R^T R$, where R is an upper triangular matrix, again with sparse structure. An equilibrated sample is then found by solving the equation $Ry = \xi$, where y is the configuration and ξ Gaussian distributed, independent random numbers. In order to remove the zero-mode in M, we attach the last site of the chain to a reference position, with an extra spring, during the factorization step but not during the ECMC simulation. This procedure allows us to generate equilibrated systems, the algorithmic complexity scaling linearly with the system size.

Influence of the initial state and quenches

We generate initial configurations equilibrated at $T/k = 1$, then run the algorithm at different temperatures, if the simulation temperature $T/k < 1$, this quenches the system. If $T/k > 1$ it is a sudden heating. We measure the distribution function $\rho_1(t,x)$ after a constant time t (corresponding to the total displacement of particles during a run), and plot the results in Fig. 1. For all changes in temperature the evolution is remarkably similar, the distribution displays the double peak structure familiar from the analytic solution of the true self-avoiding walk eq. (4). When we rescale these curves they superpose to within the displayed line width; the scaling function is insensitive to the surrounding environment. In Fig. 2 we plot the width of the distribution (root-mean-squared deviation), $\sigma^2 = \langle x^2 \rangle$, as a function of the final temperature. In this figure we scale the width by the width of a zero-temperature starting configuration propagating at $T/k = 1$, the protocol that was studied in our previous publication [6]. As temperature increases the distribution narrows.

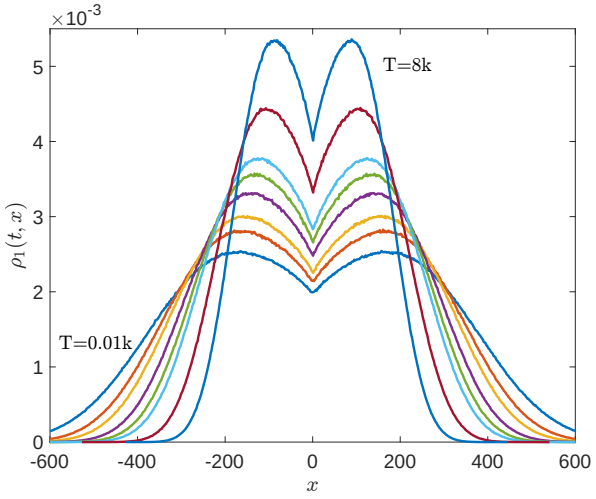

FIG. 1. A zero tension harmonic chain is prepared at temperature $T/k = 1$, ECMC simulations are then performed at: $T/k = [0.01, 0.25, 0.5, 1, 1.5, 2, 4, 8]$. Evolution, $\rho_1(t,x)$, eq. (4) for event-chain lengths of length $t = 2048$. Higher temperatures spread more slowly, giving narrower, higher curves. All curves superpose to within line width on scaling to a standard width. Data from 2^{25} configurations for each curve.

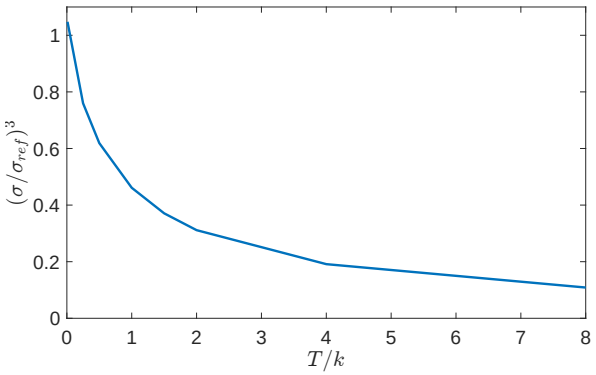

FIG. 2. Evolution of the width, σ, of distribution $\rho_1(t,x)$, eq. (4) from the data in Fig. 1. We normalized to width, σ_{ref} in a system prepared at zero temperature and then simulated at $T/k = 1$.

Exact calculations in [11] on the true self-avoiding walk indicate that if we compare the propagation of a cold start, and a hot start the ratio of widths $(\sigma_{\rm hot}/\sigma_{\rm cold})^3 = 1/2$ This corresponds to the point $(1, 1/2)$ in Fig. 2. In Fig. 3 we study $(\sigma_{\rm hot}/\sigma_{\rm cold})^3$ as a function of simulation time t to evaluate the infinite time limit of the ratio. Empirically we find a near-linear extrapolation if we plot the data as a function of $1/t^{1/4}$. We performed a non-linear fit of our data for large t to the form

$$(\sigma_{\rm hot}/\sigma_{\rm cold})^3 = \alpha_1 + \frac{\alpha_2}{t^{\alpha_3}} \tag{10}$$

using the Matlab function "nlinfit". The result is shown

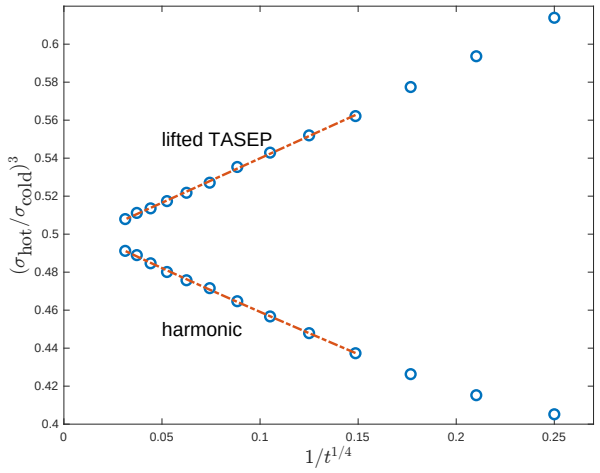

FIG. 3. Ratio of widths $\sigma_{\rm hot}$ and $\sigma_{\rm cold}$ for hot and cold starts, as a function of $t^{-1/4}$. The long-time limits extrapolate to $(\sigma_{\rm hot}/\sigma_{\rm cold})^3$ close to 1/2. Times from $t = 2^8$ to $t = 2^{20}$. Red dashed line fit to eq. (10).

as a dashed line in the Fig. 3. We find $(\alpha_1, \alpha_2, \alpha_3) = (0.507, -0.414, 0.233)$. This very slow extrapolation with time prevents us from finding a high precision result, but the results for this ratio for ECMC do seem compatible with the mathematical result for the true self-avoiding walk, $\alpha_1 = 1/2$. The linear variation in $t^{-1/4}$ in Fig. 3 is indeed compatible with the fitted exponent $t^{-0.233}$.

We performed analogous simulations for the lifted TASEP at half-filling. We compare starting configurations of either an ordered state ("cold" start) or configurations drawn from the equilibrium distribution ("hot" start). The data displays a very similar scaling as a function of simulation time giving, $(\alpha_1, \alpha_2, \alpha_3) = (0.493, 0.470, 0.251)$. Both extrapolations are rather remarkable, since the microscopic formulation of ECMC on harmonic chains, or lifted TASEP is rather different from the formulation of the true self-avoiding walk. We conclude that there is universality in scaling ratios for ECMC.

Properties of $L(t,x)$

We now study the form of the function $L(t,x)$, eq. (2), giving the number of visits of the active particle to the site at x, Fig. 4. At the top of the figure in solid blue we show the average form of this function, which is characterized by a discontinuous slope at the origin. We also separate in this figure the configurations which have moved, on average, to the left, or to the right (red and orange dash). These two contributions have a strong left-right asymmetry. Both of these functions have a *discontinuity* in their slopes at the origin, necessary for their sum to display a singularity at the origin. In the bottom panel of Fig. 4 we show a single trajectory contributing to the average distributions. Individual trajectories are extremely rough. We

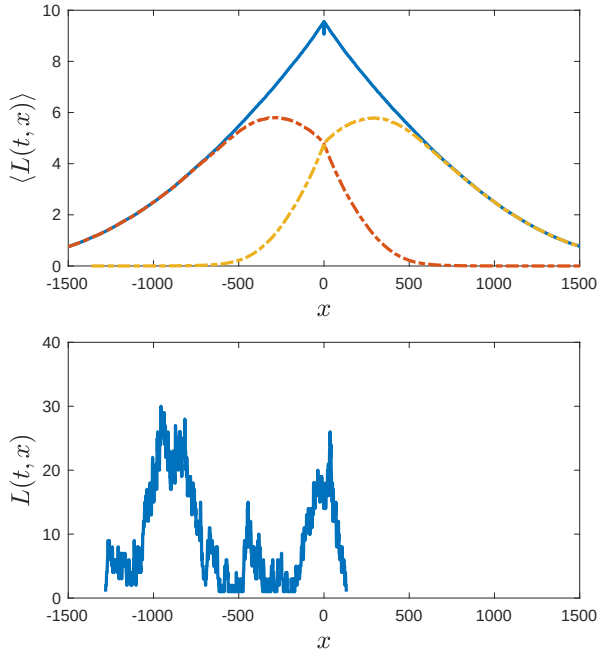

FIG. 4. Top: blue solid line, the average of the function $L(t,x)$, eq. (2) at the end of simulations of length $t = 16384$, averaged over 131072 realizations. Dashed lines, contributions to $L(t,x)$ for which the occupation was on average on the left or right. Bottom: A single trajectory contributing to $L(t,x)$. Cold start.

show a contribution that is skewed to the left compared to the starting point at $x = 0$, giving a contribution to the red dashed distribution.

We find the form of the function $L(t,x)$ rather puzzling: From the scaling form eq. (4) one is tempted to deduce that, at least in scaling form

$$L(t,x) \sim \int_{x^{3/2}}^{t} \frac{1}{t'^{2/3}}\, dt' \sim (t^{2/3} - \sqrt{x}) \qquad (11)$$

The lower cut-off in this equation corresponds to the time needed to propagate from the origin to position x. It is very natural that L is singular at the origin. However, the singularity at the origin is weaker than that predicted from this naive argument.

Stress

Let us now consider the simulation of a harmonic system with strain with the energy

$$E = \frac{k}{2} \sum_{i=1}^{N} (y_{i+1} - y_i - l_0)^2 \qquad (12)$$

with periodic boundary conditions, $y_{N+1} = y_1$. The ground state of this energy is still $y_i = \text{const}$. This corresponds to stressing each spring, by a constant value kl_0. From the results of [2, 16] this must lead to a change in

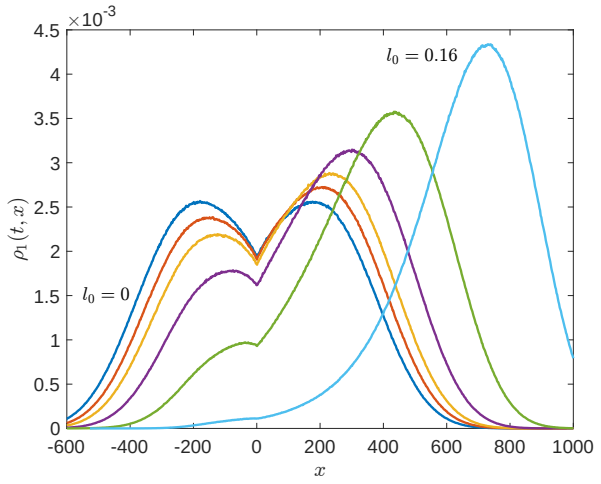

FIG. 5. Evolution of distribution, $\rho_1(t,x)$, eq. (4) with stress eq. (12) $l_0 = [0, 0.01, 0.02, 0.04, 0.08, 0.16]$. $N = 8192$, path length $t = 2048$. $T/k = 1$. Data from 2^{26} simulation for each curve.

the large-scale dynamics of the algorithm since the stress and mean displacement of the active (mobile) particle are linked. The average position of the distribution ρ_1 thus displaces with increasing l_0

We perform simulations starting with a ground state configuration $y_i = 0$ (cold start). We see Fig. 5 that imposing stress leads to a drift of the configuration to the right; we checked that the drift speed is proportional to l_0. Rather remarkably, for small to moderate values of l_0 the singularity at the origin of the curve ρ_1, remains even as the center of mass of the curve transports to the right.

GENERAL POTENTIALS

One-dimensional statistical mechanics

The statistical mechanics of a system of particles with nearest-neighbor interactions can be solved analytically in the isobaric ensemble [21]. In particular, the distribution of particle separations follows the distribution law $e^{-\beta(V(r)+p\,r)}$, where $V(r)$ is the inter-particle potential for separation r, and p the thermodynamic pressure. From this distribution, we find the average separation between particles

$$\Delta(p) = \langle r \rangle_p = \frac{\int r\, e^{-\beta(V(r)+p\,r)}\, dr}{\int e^{-\beta(V(r)+p\,r)}\, dr} \tag{13}$$

With this statistical weight, we also find the useful relations:

$$\langle r dV/dr \rangle_p + p\Delta(p) = T \tag{14}$$

$$T\rho_c - \langle dV/dr \rangle_p = p \tag{15}$$

Eq. (14) is the usual virial equation [22], that we use to verify the stress state of our chains. In eq. (15) the contact density, $\rho_c = e^{-\beta V(0)}/z_1$, with z_1 the single bond partition function. When the potential diverges at the origin, as is the case for the Lennard-Jones potential, $\rho_c = 0$, and we have an easy, independent measure of the thermodynamic pressure.

In our simulations, we use both cold and hot starts. For the cold start, we initialize with a uniformly spaced system, where we calculate, by numerical integration of eq. (13), the mean separation as a function of pressure: and place particles uniformly, with a total system length of $L = N\Delta(p)$. We then use the imposed p as the value of the factor field in our simulations.

For the hot start (where a sample is pre-equilibrated) before each simulation we generate a library of 10^8 samples according to the distribution of eq. (13) using Chebyshev interpolation to implement inverse transform sampling [23]. From this library of separations we generate large numbers of initial states needed to calculate the distributions $\rho_1(t,x)$ and $\rho_2(t,x)$ by randomly drawing a series of N values of r from this library. We expect that differences from the isobaric and constant length ensembles are small for the large system sizes that we simulate.

Longer range interactions

There is no closed-form expression for the properties of one-dimensional chains with interactions beyond the first-nearest neighbor. It is not possible to generate pre-equilibrated samples as above. We can still, however, use the virial theorem to express the pressure in terms of the potential. We specialize to the case of first and second-nearest neighbor interactions. We have:

$$pL = NT + \sum_{i<j} r_{ij} f_{ij} \tag{16}$$

where $r_{ij} = r_i - r_j$, with the nearest image convention and f_{ij} is the force on i from j. Let us now introduce factor fields p_1 and p_2, between first and second-nearest neighbors, so that the nearest neighbor interaction becomes $V_1(r) + p_1\, r$. We find from the virial theorem with the modified potentials:

$$(L/N)p = T + \langle r^{(1)} f_1 + r^{(2)} f_2 \rangle - (L/N)(p_1 + 2p_2) \tag{17}$$

where $f_i(r) = -dV_i(r)/dr$, and $r^{(i)}$ the corresponding separation vector. We anticipate that the zero drift criterion for the distribution $\rho_1(t,x)$, then corresponds to $p = p_1 + 2p_2$. While the zero-drift criterion gives a unique criterion for the factor field with nearest neighbor interactions, this is no longer the case when longer-ranged interactions are present. We explore numerically the dynamics to determine the efficiency of algorithms with different choices of p_1 and p_2. In particular, we make a detailed study with repulsive exponential interactions.

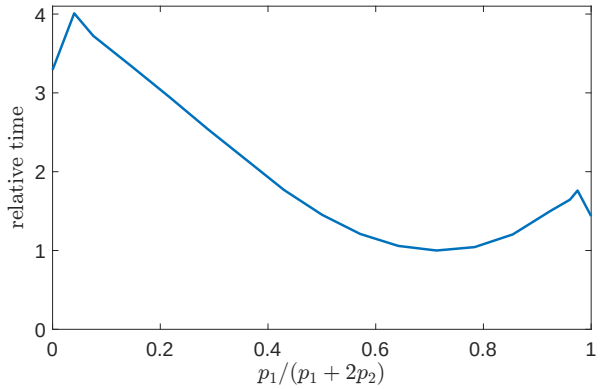

FIG. 6. Autocorrelation times of chain with first and second-nearest neighbor exponential potentials, on the line $p = p_1 + 2p_2$. Simulation time, $t = 2^{29}$, $N = 8096$.

We generalize the result of eq. (15) using the methods of [24]. We consider a chain of N particles with first and second-nearest neighbor interactions V_1, V_2. We then shorten the chain by ϵ. Clearly $\beta p = -\partial \ln Z/\partial\epsilon$. We implement this shortening by removing a slice in configuration space between 0 and ϵ. We hold a single $i = 1$ particle at $r = 0$, to fix the center of mass of the chain. Then, the integral over the particle $i = 2$ becomes,

$$\int_\epsilon^{r_3} dr_2 \, \exp\left(-\beta V(r_2 - r_1 - \epsilon)\right)$$

With a similar modification for the interaction with the second-nearest neighbors. Keeping variations to order ϵ we find

$$p = T\rho_c - \left\langle \frac{\partial V_1}{\partial r} \right\rangle - 2\left\langle \frac{\partial V_2}{\partial r} \right\rangle$$

The factor of two is because shortening a single nearest neighbor separation modifies the distance between two particles at second-nearest neighbor. The term in ρ_c comes from the disappearance of configurations at contact between the particles $i = 1$ and $i = 2$.

Exponential interactions

We consider the case of repulsive interactions between particles of the form $V(r) = a\exp(-|r|/\ell)$ and systems with first and second-neighbor interactions. To implement the event-chain algorithm, with a factor field we need to find the solution, r, to the equation

$$a\exp(-r/\ell) + pr = \Delta E \tag{18}$$

ΔE, is calculated from the difference between V and V^+, together with the thermal activation. Solutions to eq. (18) are found from the Lambert W function [25], defined as solutions to the equation

$$We^W = z \tag{19}$$

We study two points with this interaction. Firstly, we confirm that the functions $\rho_1(t, x)$ and $\rho_2(t, x)$ measured in simulations with more general interactions remain compatible with those found with the true self-avoiding walk. Secondly, how can one efficiently implement the factor-field method in systems with longer-range interactions? Let us emphasize that the factor-field method, as previously studied, introduces a linear potential between nearest-neighbor interacting particles, with an amplitude that is equal to the thermodynamic pressure. It is at this unique point that the method is the most efficient. With more general interactions there is potentially a line of solutions $p_1 + 2p_2 = p$, where p_i is the factor field with the $i'th$ neighbor and p is again the thermodynamic pressure. To generate an efficient algorithm are there further constraints on the individual amplitudes p_i?

We implemented the simulations with $a = 20$, for nearest neighbor interactions and $a = 40$, for second-nearest interactions, with $\ell = 2$, $T = 0.3$, $L = 4.69703N$, $N = 8192$. With these parameters, there are large contributions to the thermodynamic pressure from first- and second-nearest neighbors on the chain. We are working at a low temperature where ECMC without factor fields becomes slow. Preliminary simulations without factor fields are used to estimate the thermodynamic pressure from the virial theorem. We equilibrate the system and then calculate the autocorrelation time of the lowest Fourier mode of the density. We then perform simulations along the line $p_1 + 2p_2 = p$. The dynamics are characterized by the universal scaling forms, eq. (4, 5); this remains true even for the extreme cases $p_1 = 0$ or $p_2 = 0$.

When measured in terms of the Monte Carlo time t (equal to the total displacement of particles) the efficiency of the code is almost independent of the exact mix between p_1 and p_2, however, extreme choices give rise to small steps before generating a collision event, so that the clock time of a simulation is sensitive to the exact mix of fields. In Fig. 6 we plot a relative clock time (compared to the best mix of fields) as a function of $p_1/(p_1+2p_2)$, demonstrating a relatively broad minimum for the autocorrelation time, in units of wall clock time. Note the two end points for $p_1 = 0$, and $p_2 = 0$ deviate from the main curve, since fewer evaluations of the Lambert W function are required. We conclude that the universal scaling form remains stable with interactions that go beyond nearest neighbor and that the efficiency of ECMC depends only weakly on the exact field values if the factor fields are tuned correctly to the thermodynamic pressure.

Lennard-Jones systems at low densities

We implemented factor-field simulations of particles with nearest-neighbor Lennard-Jones interactions. A previous paper [16] reported the properties of this system at high densities, such that the average separation between particles is smaller than the position of the potential minimum. We here study the properties of a system in which

FIG. 7. Equilibrated Lennard-Jones configuration at a low density, showing well-separated clusters. $\beta\epsilon = 2$, $\beta p = 0.03$, $N = 96$ particles, mean separation. $\Delta = 4.007$.

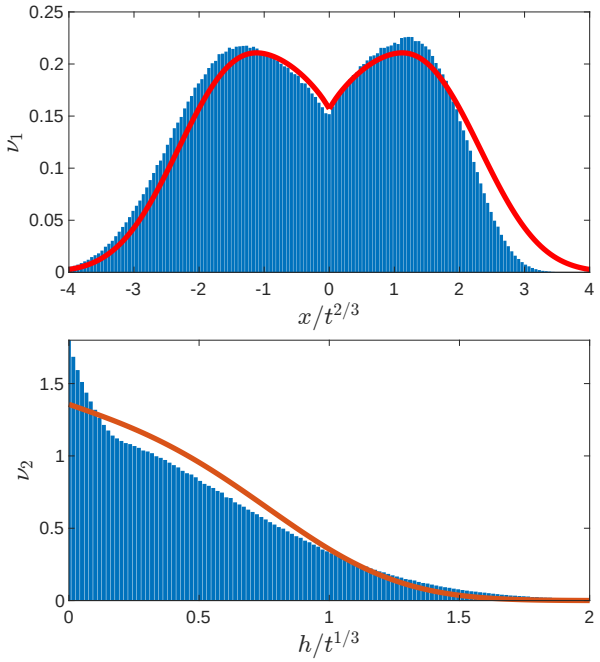

FIG. 8. Plots of the scaling functions ν_1 and ν_2, eqs. (4, 5) for a cold start with simulation time $t = 1024$, parameters correspond to Fig. 7. For short times $\rho_1(t, x)$ has a clear back-forwards asymmetry, which only slowly decays for longer simulation times, Fig. 9. $\rho_2(t, h)$ has a pronounced peak for small h. Red, solid lines the analytic solution to the true self-avoiding walk eq. (4, 5) Blue histogram: binned data from simulation.

$\beta p = 0.03$, $\Delta = 4.007$, and for which $\epsilon\beta = 2$, where ϵ is the well depth. Length units are set by the Lennard-Jones potential which crosses $E = 0$ for unit separation. As seen in Fig. 7 for these parameters the system breaks up into a series of isolated clusters. The ECMC algorithm must equilibrate the internal structure of the clusters, as well as "jump" the activity between clusters. The question is then whether the large-scale dynamics of this heterogeneous system still converge to the universal forms of [6, 11], eq. (4, 5)

Implementation of the factor-field algorithm for the Lennard-Jones potential requires solving equations of the form

$$\frac{1}{r^{12}} - \frac{1}{r^6} + pr = \Delta E \qquad (20)$$

for r. We proceed by using an iterative solver, based on Halley iteration [25], a higher-order generalization of Newton-Raphson. From an initial guess of the root it requires typically four iterations to fully converge the solution of eq. (20) to machine precision.

We find that the "hot", pre-equilibrated samples generate a symmetric function $\rho_1(t, x)$ in agreement with eq (4). However, the cold samples generate a small back-forward asymmetry for $\rho_1(t, x)$, Fig. 8. The distribution of $\rho_2(t, x)$ differs considerably from the analytic form Fig. 8, with a strong peak for small h. This implies that if one stops the simulation one has visited the final site less often than would be expected from the statistics of the true self-avoiding walk.

We study the skewness of the distribution $\rho_1(t, x)$, Fig. 9 bottom, as a function of simulation time t, where the skewness is defined as a normalized third moment:

$$\text{skew} = \langle (x - \langle x \rangle)^3 \rangle / \sigma^3 \qquad (21)$$

We find that eq. (21) decays only very slowly with t, and possibly at the largest times decays as skew $\sim t^{-1/3}$, which is similar to the asymmetry found in the lifted TASEP model [17]. Despite the slow decay of the skewness of the distribution to zero we find that the width of the distribution, σ, Fig. 9 top, fits the exponent 2/3 from eq. (4) even for short times. Despite showing very slow convergence in time, we conclude that even this heterogeneous system does display the universal true self-avoiding form.

MIXING TIMES

Until now, we have used autocorrelation times as a measure of the efficiency of a simulation algorithm. However, when starting from an arbitrary configuration one should also have some idea of mixing times, which bound the time for samples generated by the simulation to be close to equilibrium, after starting in an arbitrary state. Certainly, in physical applications there are many examples involving nucleation, where this time can be much larger than autocorrelation times. For one-dimensional models with factor-field accelerated ECMC we showed [16] that a system of hard rods, which has an autocorrelation time for density fluctuations scaling as $N^{3/2}$ has an asymptotically slower mixing time scaling as N^2. This is for a configuration where all particles start in contact, and relaxation of the configuration only occurs by loss of particles from the end of a dense starting state. Can one make similar statements for the simulation of models such as the chains considered in this paper? For simplicity, we will only consider configurations of the harmonic chain, to avoid considering configurations such as that displayed in Fig. 7 where the use of very deep Lennard-Jones potentials and very low densities must lead to slow coarsening dynamics.

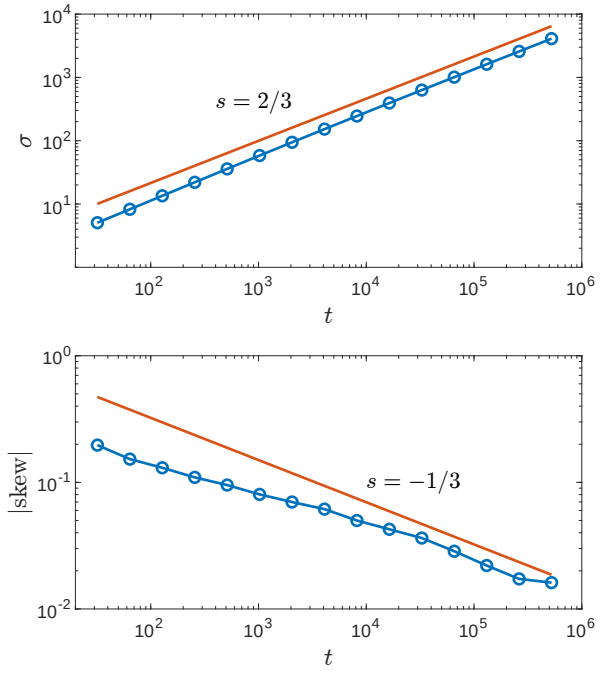

FIG. 9. Top: evolution of the width, σ, of the distribution of ρ_1 as a function of simulation time t. Red line a guide to the eye with exponent $s = 2/3$. Bottom, evolution of the skew with simulation time t. Red line exponent $s = -1/3$ guide to eye. System corresponds to Fig. 7. Data from 2^{22} configurations per point.

We proceed by studying trial configurations, that are far from equilibrium, and make analytic arguments which we confirmed with numerical studies. We start with an analogue of the dense configurations that have the largest mixing times for hard rods:

$$\begin{aligned} y_i &= a \qquad 1 \le i \le \lfloor N/2 \rfloor \\ &= -a \qquad \text{otherwise} \end{aligned} \tag{22}$$

$\lfloor\ \rfloor$ denotes the integer part and $a > 0$ is an amplitude. On starting the position of the active particle at random it will take a time $O(N^{3/2})$ to find the region where $y_i < 0$. For $a^2 k \gg T$ the active particle then remains confined to regions with $y_i < 0$ while making steps of amplitude $O(\sqrt{T/k})$. Thus, it takes a time $O(aN\sqrt{k/T})$ to erase the step in the initial configuration with ECMC. If $a^2 \gg NT/k$ then this time is longer than the autocorrelation time. We can easily build configurations for which the mixing time is unbounded. The case $a^2 = NT/k$ is interesting. It corresponds to injecting energy $O(NT)$ into the chain; comparable to the thermal energy at equilibrium. This motivates two questions.

- (1) Are there configurations with energy $\gg NT$ that nevertheless mix rapidly?

- (2) Are there configurations with an energy budget $O(NT)$ that mix more slowly than eq. (22)?

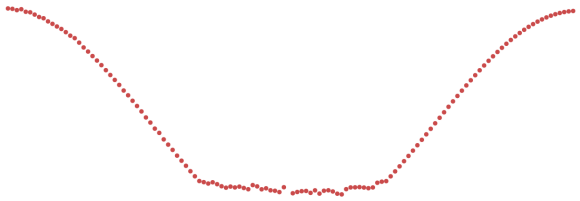

FIG. 10. Initial configuration is chosen as eq. (24). The algorithm has driven the active particle to the central part of the configuration, which filled in with a local state which is close to equilibrium. When the ECMC has erased the whole initial state we find a bound on the mixing time.

To answer case (1) we consider the configuration

$$\begin{aligned} y_i &= a \qquad i \text{ odd} \\ y_i &= -a \qquad i \text{ even} \end{aligned} \tag{23}$$

The energy is unbounded for large amplitude a. When the particle activity falls on an "even" site the particle can make a move at once to $y = O(+a)$ and can explore the whole chain in a time $O(N^{3/2})$ independent of the value of a. Thus, there are configurations with arbitrarily high energy with fast mixing.

For case (2) we consider the configuration

$$y_i = N\sqrt{T/k}\cos\left(2\pi i/N\right) \tag{24}$$

The algorithm advances by motion of particles a distance $O(\sqrt{T/k})$, and the energy of this configuration is $O(NT)$. On starting at an arbitrary position the ECMC algorithm runs "downhill" to the smallest values of y_i, Fig. 10, and starts moving the particles with smallest y_i in a positive direction, "filling in" the bottom of the cosine. To erase the initial configuration requires moving each of the N particles a distance $O(N\sqrt{T/k})$. Thus, we have a lower bound on mixing time of N^2, when we require that the energy $O(NT)$ in the initial state, as was found for the hard-rod problem.

BREAKING BALANCE

Given the similarity of ECMC to active matter, with driven trajectories, it is interesting to modify the dynamics in such a way that driven states are no longer compatible with the Boltzmann distribution. Are the notable features that we recognize for the true self-avoiding walk still present in such fully non-equilibrium systems? We choose to do this by modifying the interactions in the harmonic chain in such a way that they are non-longer reciprocal [26], that is when the force from i to $i+1$, is different from the force for $i+1$ to i. We modify the form eq. (9) so that in the collision rules eq. (7) different constants k_r and k_l are used for interactions to the right and to the left of the active particle. We perform simulations for several values of k_r/k_l and plot the results in Fig. 11. It is not surprising that distribution $\rho_1(t, x)$ drifts

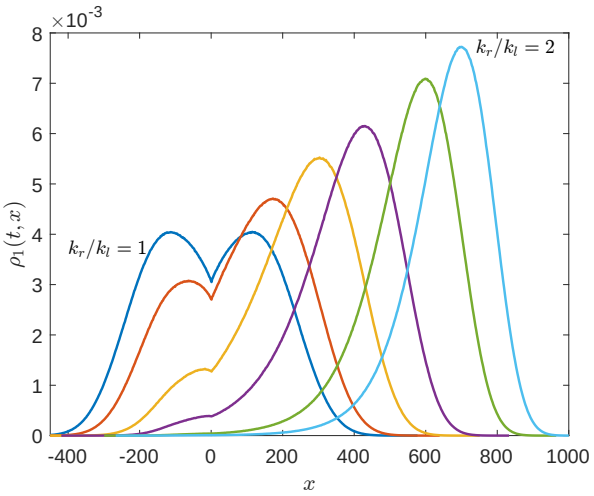

FIG. 11. Plots of $\rho_1(t,x)$ for a dynamical system that breaks global balance for ratios $k_r/k_l = [1, 1.1, 1.3, 1.5, 1.8, 2]$, $t = 2048$, $T/k_l = 1$.

like Fig. 5. Remarkably, the evolution again conserves a singularity at $x = 0$. We have no explanation as to the origin and the stability of this singularity under several forms of perturbation of the true self-avoiding walk.

CONCLUSIONS

We have studied variants of the ECMC including factor fields and compared with an exactly soluble model of polymer growth. We find that the distribution functions, which were studied in detail in [6] for a harmonic chain, remain valid even for physical systems that are strongly heterogeneous, such as the Lennard-Jones chain of Fig. 7. Introducing tension however leads to very different distribution functions. It is remarkable however that the singularity at the origin in the function $\rho_1(t,x)$, remains even as the average position drifts. We note that some consideration has been given to drift in the paper [27]. We have no explanation as to why this is so. Similar singularities remain even when breaking global balance.

ACKNOWLEDGMENTS

I thank Werner Krauth for extensive discussions on non-reversible simulations and lifted TASEP.

CODE

C++ code for simulating the exponential and Lennard-Jones interactions, available from https://github.com/acmaggs/acmaggs.github.io.

REFERENCES

[1] E. P. Bernard, W. Krauth, and D. B. Wilson, Event-chain Monte Carlo algorithms for hard-sphere systems, Phys. Rev. E **80**, 056704 (2009).

[2] M. Michel, S. C. Kapfer, and W. Krauth, Generalized event-chain Monte Carlo: Constructing rejection-free global-balance algorithms from infinitesimal steps, The Journal of Chemical Physics **140**, 054116 (2014), https://pubs.aip.org/aip/jcp/article-pdf/doi/10.1063/1.4863991/15472076/054116_1_online.pdf.

[3] E. P. Bernard and W. Krauth, Two-step melting in two dimensions: First-order liquid-hexatic transition, Phys. Rev. Lett. **107**, 155704 (2011).

[4] M. Engel, J. A. Anderson, S. C. Glotzer, M. Isobe, E. P. Bernard, and W. Krauth, Hard-disk equation of state: First-order liquid-hexatic transition in two dimensions with three simulation methods, Phys. Rev. E **87**, 042134 (2013).

[5] S. C. Kapfer and W. Krauth, Irreversible local Markov chains with rapid convergence towards equilibrium, Phys. Rev. Lett. **119**, 240603 (2017).

[6] A. C. Maggs, Non-reversible Monte Carlo: An example of "true" self-repelling motion, Europhysics Letters **147**, 21001 (2024).

[7] D. J. Amit, G. Parisi, and L. Peliti, Asymptotic behavior of the "true" self-avoiding walk, Phys. Rev. B **27**, 1635 (1983).

[8] L. Peliti, Self-avoiding walks, Physics Reports **103**, 225 (1984).

[9] R. Rammal, J. C. A. d'Auriac, and A. Benott, Statistics of the true self-avoiding walk in one dimension, Journal of Physics A: Mathematical and General **17**, L9 (1984).

[10] .

[11] L. Dumaz and B. Tóth, Marginal densities of the "true" self-repelling motion, Stochastic Processes and their Applications **123**, 1454 (2013).

[12] B. Tóth, The "True" Self-Avoiding Walk with Bond Repulsion on $\mathbb{Z}$: Limit Theorems, The Annals of Probability **23**, 1523 (1995).

[13] B. Tóth and B. Valkó, Perturbation of singular equilibria of hyperbolic two-component systems: A universal hydrodynamic limit, Communications in Mathematical Physics **256**, 111 (2005).

[14] E. Kosygina and J. Peterson, Convergence of rescaled "true" self-avoiding walks to the tóth-werner "true" self-repelling motion (2025), arXiv:2502.10960 [math.PR].

[15] E. Schertzer, R. Sun, and J. M. Swart, The brownian web, the brownian net, and their universality, in *Advances in Disordered Systems, Random Processes and Some Applications*, edited by P. Contucci and C. Giardinà (Cambridge University Press, 2016) p. 270–368.

[16] Z. Lei, W. Krauth, and A. C. Maggs, Event-chain Monte Carlo with factor fields, Phys. Rev. E **99**, 043301 (2019).

[17] F. H. L. Essler and W. Krauth, Lifted tasep: A solvable paradigm for speeding up many-particle Markov chains, Phys. Rev. X **14**, 041035 (2024).

[18] M. F. Faulkner, L. Qin, A. C. Maggs, and W. Krauth, All-atom computations with irreversible Markov chains, The Journal of Chemical Physics **149**, 064113 (2018), https://pubs.aip.org/aip/jcp/article-pdf/doi/10.1063/1.5036638/13501056/064113_1_online.pdf.

[19] M. Michel, *Irreversible Markov chains by the factorized Metropolis filter : algorithms and applications in particle systems and spin models*, Ph.D. thesis (2016), thèse de doctorat dirigée par Krauth, Werner Physique Paris Sciences et Lettres (ComUE) 2016.

[20] R. M. Corless, G. H. Gonnet, D. E. G. Hare, D. J. Jeffrey, and D. E. Knuth, On the Lambert W function, Advances in Computational Mathematics **5**, 329 (1996).

[21] R. Feynman, *Statistical mechanics: a set of lectures*, Frontiers in physics : a lecture note and reprint series (Sarat Book Distributors, 1972).

[22] A. Maggs, The virial theorem with periodic boundary conditions, Chemical Physics Letters **816**, 140389 (2023).

[23] T. A. Driscoll, N. Hale, and L. N. Trefethen, *Chebfun Guide* (Pafnuty Publications, 2014).

[24] B. Li, Y. Nishikawa, P. Höllmer, L. Carillo, A. C. Maggs, and W. Krauth, Hard-disk pressure computations-a historic perspective, The Journal of Chemical Physics **157**, 234111 (2022), https://pubs.aip.org/aip/jcp/article-pdf/doi/10.1063/5.0126437/16715104/234111_1_online.pdf.

[25] Boost C++ libraries (2024), https://www.boost.org/doc/libs/1_86_0/libs/math/doc/html/root_finding.html.

[26] M. Fruchart, R. Hanai, P. B. Littlewood, and V. Vitelli, Non-reciprocal phase transitions, Nature **592**, 363 (2021).

[27] A. Erschler, B. Tóth, and W. Werner, Some locally self-interacting walks on the integers, in *Probability in Complex Physical Systems*, edited by J.-D. Deuschel, B. Gentz, W. König, M. von Renesse, M. Scheutzow, and U. Schmock (Springer Berlin Heidelberg, Berlin, Heidelberg, 2012) pp. 313–338.